

EFFECT OF HEAT TREATMENTS ON THE TENSILE PROPERTIES OF ADDITIVELY MANUFACTURED 15-5 PH STAINLESS STEEL

Rukesh Gusain^{1,2}, Paul R. Gradl³, Shuai Shao^{1,2}, Nima Shamsaei^{1,2*}

¹National Center for Additive Manufacturing Excellence (NCAME), Auburn University, Auburn, AL 36849, USA

²Department of Mechanical Engineering, Auburn University, Auburn, AL36849, USA

³NASA Marshall Space Flight Center, Propulsion Department, Huntsville, AL 35812, USA

*Corresponding author:

Email: shamsaei@auburn.edu

Phone: (334) 844 4839

Abstract

This study investigated the effect of post-manufacture heat treatments on the microstructure and mechanical properties of 15-5 PH stainless steel (SS) fabricated by laser powder-directed energy deposition (LP-DED). Various heat treatment procedures (CA-H900 and CA-H1150) were conducted to evaluate their effects on the tensile behavior of LP-DED 15-5 PH SS. Scanning electron microscopy was used to characterize the microstructural features and the fracture surfaces. Tensile tests were performed to evaluate the mechanical properties at cryogenic and room temperatures. The mechanical behavior of the LP-DED 15-5 PH SS in different heat treatment conditions is discussed based on their microstructures and fracture surfaces. Reduction in area of CA-H1150 treated specimens after tensile tests was significantly higher than CA-H900 ones, while the ultimate tensile and yield strengths of CA-H900 specimens were higher compared to the CA-H1150 ones. The CA-H1150 specimens had relatively coarser Cu-enriched precipitates, and exhibited greater necking compared to CA-H900 specimens.

Keywords: Laser powder directed energy deposition (LP-DED), precipitation hardened stainless steel, heat treatment effects, cryogenic temperature, tensile fracture

Introduction

15-5 PH stainless steel (SS) is a martensitic stainless steel known for its excellent mechanical properties and corrosion resistance at various temperatures [1,2]. This alloy is typically used to manufacture components in aerospace industries, nuclear reactors, and medical applications where the service temperature ranges from cryogenic to elevated [3]. Since components used in such sectors often possess intricate geometries which are difficult and time-consuming to be manufactured via traditional subtractive manufacturing, additive manufacturing (AM) offers a viable solution. One of the AM techniques is laser powder-directed energy deposition (LP-DED), in which a laser beam is used to melt the powder delivered by an inert carrier gas through nozzles.

However, the mechanical behaviors of parts manufactured by AM techniques differ from those fabricated via traditional manufacturing techniques due to residual stresses and process-induced defects such as lack of fusion, keyholes, and gas-entrapped pores [4–7]. In addition, AM parts tend to have different microstructures than wrought ones, which often remain even after applying the same thermal post-processing techniques [8–10]. While a few research articles investigated the effects of build orientations, heat treatments and surface treatments on microstructural features and mechanical properties of additively manufactured 15-5 PH SS [2,11–18], there still exists a knowledge gap regarding the effect of heat treatments on tensile properties and the tensile fracture mechanisms at different temperatures. This study aims to investigate the effects of heat treatments on the microstructure and tensile behaviors of LP-DED 15-5 PH SS at cryogenic and room temperatures.

Experimental Details

Argon atomized 15-5 PH SS powder supplied by Praxair Surface Technologies was used to fabricate the cylindrical bars (diameter = 11mm) by LP-DED technique in RPM Innovations (RPMI) 557 machine. The detailed chemical composition of this powder is listed in **Table 1**. The cylindrical bars were fabricated using a process parameter set, laser power of 1070 W, layer height of 0.38 mm, laser scan speed of 1016 mm/min, and powder feed rate of 15.2 g/min under the argon environment.

After fabrication, the cylindrical bars were stress-relieved at 650°C for an hour which was followed by hot isostatic pressing (HIP) at a temperature and pressure of 1163°C and 103MPa for 3 hours, respectively. The bars underwent solution treatment at 1050°C for half an hour (i.e., Condition A (CA)). After that, the specimens were divided into two groups: one was aged at 482°C for an hour (i.e., H900), known as the peak-age condition, and the other was over-aged at 621°C for 4 hours (i.e., H1150). Both non-heat treated (NHT) and heat treated LP-DED 15-5 samples were cut at the gage section in the planes parallel to (i.e., longitudinal plane) and perpendicular to (i.e., radial plane) the build direction (BD). These samples were mounted and polished for microstructural characterization. A Zeiss Crossbeam 550 scanning electron microscope (SEM) was used to characterize the microstructure of the samples in both radial and longitudinal directions. The fully heat treated specimens were then machined to final geometries, as shown in **Figure 1** for tensile tests.

The machined LP-DED 15-5 PH SS specimens were subjected to quasi-static monotonic tensile tests on MTS servo-hydraulic testing machines with 100kN load cells. The tensile specimens were loaded at a strain rate of 0.005mm/mm/min at temperatures of -196°C and 21°C. These tests were conducted following the ASTM E8-21 standard for room temperature and the ASTM E21-20 standard for cryogenic temperature. Extensometers were installed in the gauge section of test specimens to measure the strain. For cryogenic tests, the specimens and grips of the machine were submerged in liquid nitrogen and soaked for 5 minutes after the specimens were cooled down to -196°C. The specimens were then loaded to failure. After completion of the tests, the fractured specimens were removed from a liquid nitrogen container. The fracture surfaces were cleaned in an ultrasonic cleaner and were analyzed using an SEM.

Table 1. Chemical composition of 15-5 PH SS powder used in this study.

Elements	Weight %
Fe	Bal.
Cr	14.99
Ni	5.24
Cu	3.5
Mn	0.49
Si	0.04
Nb	0.2
O	0.03
Mo	0.01
N	0.01
C	0.01
P	0.006
S	0.003
Other	0.1

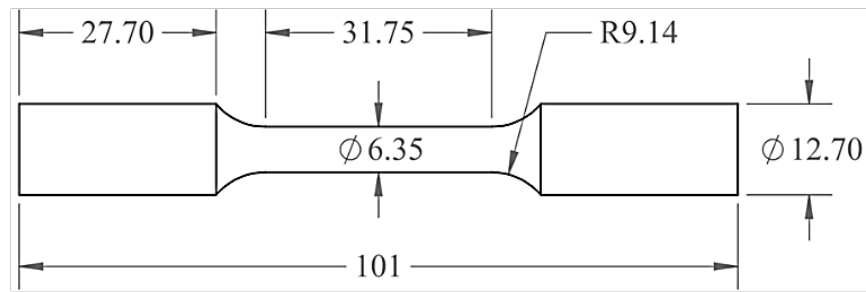


Figure 1. Tensile specimen geometry of LP-DED 15-5 PH SS (All dimensions are in mm).

Results and Discussion

The inverse pole figure (IPF) maps obtained after electron backscatter diffraction (EBSD) analysis on the longitudinal planes of NHT, CA-H900, and CA-H1150 samples are shown in **Figure 2**. These EBSD analyses also showed the presence of a minimal fraction of retained austenite in the martensitic matrix. The fraction of retained austenite in NHT, CA-H900, and CA-H1150 samples was 0.1%, 0.1%, and 0.14%, respectively. Due to the high cooling rate during the AM process, the austenitic phase gets transformed into martensite. The formation of retained austenite might be because of the diffusion of austenite stabilizing elements (i.e., Cu, Ni) into the grain boundaries, which may have acted as nucleation sites for austenite grains [19]. The slightly higher fraction of retained austenite in the CA-H1150 sample could be because of the longer aging duration at a temperature close to the austenite reversion temperature [19].

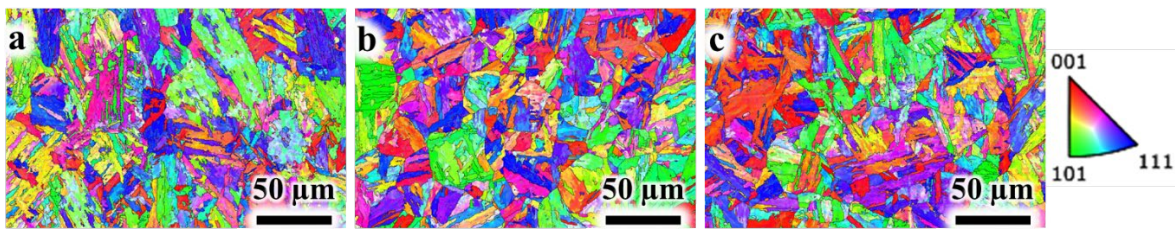


Figure 2. IPF maps obtained from the longitudinal planes of a) NHT b) CA-H900 and c) CA-H1150 samples of LP-DED 15-5 PH SS.

The elemental maps obtained after energy dispersive X-ray spectroscopy (EDS) analysis on CA-H900 and CA-H1150 samples are presented in **Figure 3** and **Figure 4**, respectively. Nano-sized Cu-enriched precipitates can be observed in the elemental maps of the CA-H900 sample, whereas the Cu-enriched precipitates were coarser in CA-H1150 samples. In addition to Cu-enriched precipitates, Cr-, Mn-, Mo-, and Nb-enriched precipitates were observed in both CA-H900 and CA-H1150 samples. Moreover, significant segregation of Ni can be observed in the CA-H1150 sample.

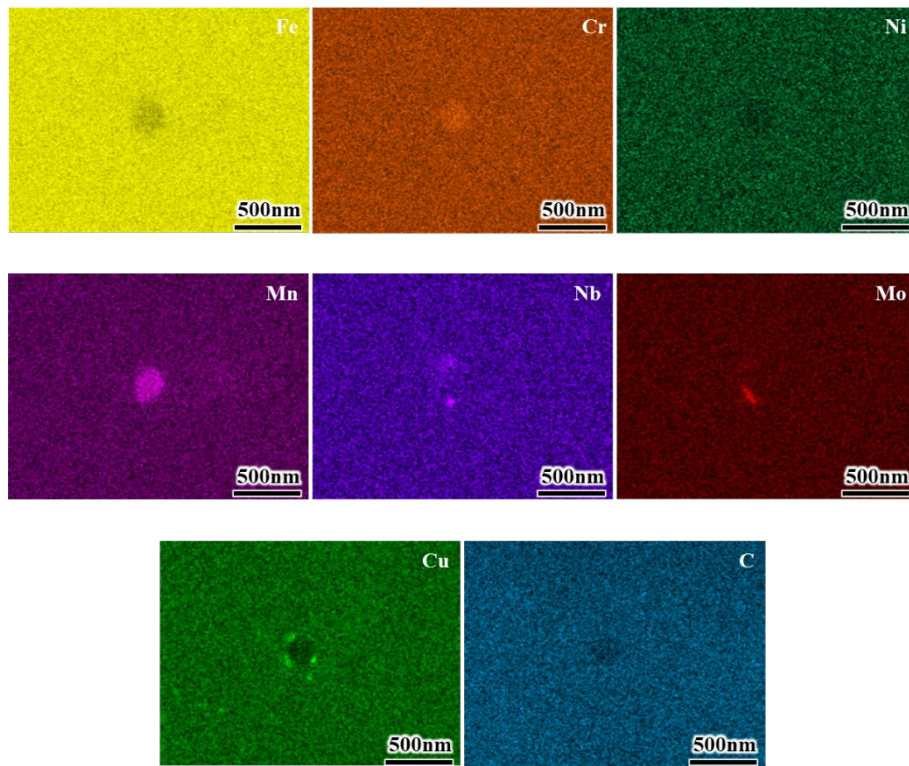


Figure 3. Elemental maps obtained from EDS analysis on a CA-H900 sample.

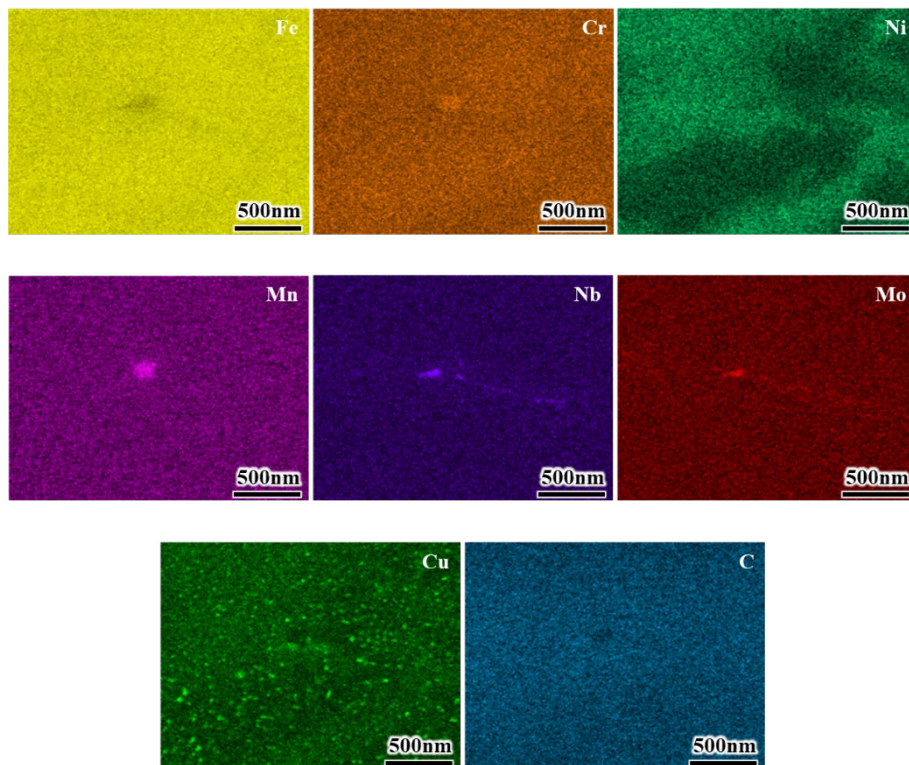


Figure 4. Elemental maps obtained from EDS analysis on a CA-H1150 sample.

The ultimate tensile strength (UTS), yield strength (YS), and reduction in area (RA) at cryogenic and room temperatures for CA-H900 and CA-H1150 specimens are shown in **Figure 5**. Compared with CA-H1150 specimens, CA-H900 specimens exhibited higher tensile strength and lower ductility. The higher strength of CA-H900 specimens can be attributed to finer Cu-enriched precipitates. These coherent finer precipitates can impede the dislocation motion more effectively, strengthening the alloy. However, upon over-aging, these precipitates coarsen. The coarsened Cu-enriched precipitates lose coherency with the matrix, decreasing the alloy's strength

[1,20]. The tensile strengths of both CA-H900 and CA-H1150 specimens were higher at the cryogenic temperature than at room temperature. At such a low temperature, the kinetic energy is not sufficient enough to exceed the activation energy required for the dislocation motion.[10,21].This reduced dislocation mobility makes plastic deformation difficult [3,22].

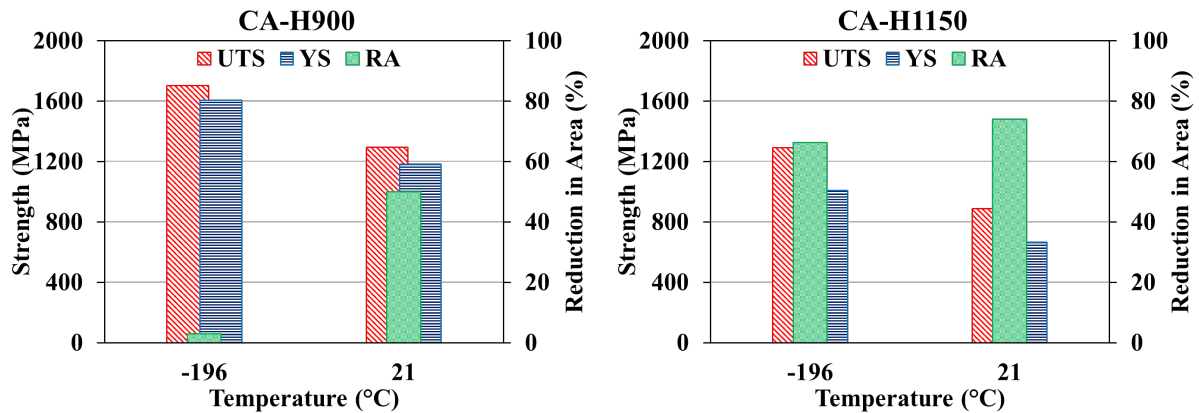


Figure 5. Bar plots showing UTS, YS and RA at cryogenic and room temperature for CA-H900 and CA-H1150 specimens.

The fracture surfaces for CA-H900 and CA-H1150 specimens tested at cryogenic and room temperatures are shown in **Figure 6**. The fracture surfaces of the CA-H900 specimens tested at cryogenic temperature had multiple facets and showed no necking, indicating transgranular brittle fracture. The CA-H900 specimens tested at room temperature exhibited slight necking, dimples, and facets on the fracture surfaces indicating a mixed-mode fracture. The fracture surfaces of the CA-H1150 specimen tested at cryogenic temperature also had features similar to CA-H900 specimens tested at the room temperature. However, at room temperature, the CA-H1150 specimens exhibited significant necking compared to the ones tested at -196°C. The presence of larger dimples on the fracture surface suggests more ductile fracture at room temperature for CA-H1150 specimens. In general, the CA-H1150 specimens exhibited greater extent of necking with larger dimples on the fracture surfaces when compared with the CA-H900 specimens.

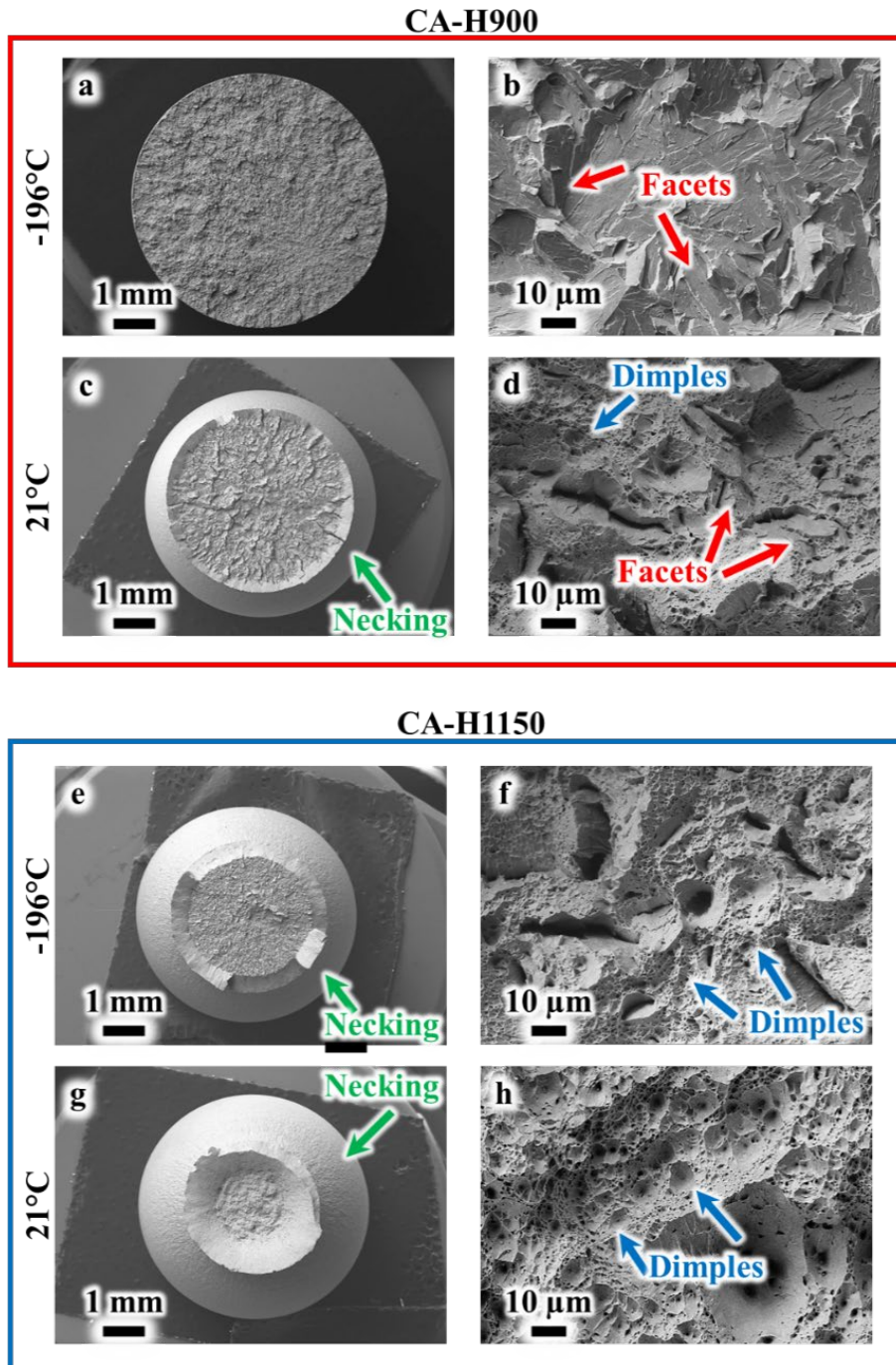


Figure 6. Tensile fracture surfaces of CA-H900 and CA-H1150 specimens at (a,b,e,f) -196°C and (c,d,g,h) 21°C .

Conclusions

This study investigated the effect of heat treatments on the tensile properties of LP-DED 15-5 PH SS at cryogenic and room temperature. The following conclusions can be drawn from this study:

- Both non-heat treated and heat treated LP-DED 15-5 PH SS possessed martensitic microstructure with a minimal fraction of retained austenite. The fraction of retained austenite was higher in CA-H1150 samples due to longer aging at a temperature closer to austenite reversion temperature.
- After full heat treatments, Cu-enriched nano precipitates were observed in the martensitic matrix. The specimens treated with CA-H1150 had coarser Cu-enriched precipitates compared to CA-H900 specimens due to longer aging at a temperature closer to austenite reversion temperature.
- The CA-H1150 specimens exhibited lower tensile strength and higher ductility than the CA-H900 specimens, which could be because of coarsened Cu-enriched precipitates.
- CA-H900 specimens exhibited brittle fracture behavior at cryogenic temperature, whereas the fracture mechanism switched to ductile-brittle mode at room temperature. In contrast, CA-H1150 specimens showed ductile-brittle mode fracture behavior at cryogenic temperature and ductile fracture behavior at room temperature.

Acknowledgement

This study is partially supported by the National Aeronautics and Space Administration (NASA) under Cooperative Agreement No. 80MSFC19C0010. This paper describes objective technical results and analysis. Any subjective views or opinions that might be expressed in the paper do not necessarily represent the views of the NASA or the United States Government.

References

- [1] Habibi Bajguirani HR. The effect of ageing upon the microstructure and mechanical properties of type 15-5 PH stainless steel. *Materials Science and Engineering: A* 2002;338:142–59. [https://doi.org/10.1016/S0921-5093\(02\)00062-X](https://doi.org/10.1016/S0921-5093(02)00062-X).
- [2] Sarkar S, Mukherjee S, Kumar CS, Kumar Nath A. Effects of heat treatment on microstructure, mechanical and corrosion properties of 15-5 PH stainless steel parts built by selective laser melting process. *J Manuf Process* 2020;50:279–94. <https://doi.org/10.1016/J.JMAPRO.2019.12.048>.
- [3] Palanisamy D, Senthil P. A comparative study on machinability of cryo-treated and peak aged 15Cr-5Ni precipitation hardened stainless steel. *Measurement* 2018;116:162–9. <https://doi.org/10.1016/J.MEASUREMENT.2017.11.008>.
- [4] Shamsaei N, Yadollahi A, Bian L, Thompson SM. An overview of Direct Laser Deposition for additive manufacturing; Part II: Mechanical behavior, process parameter optimization and control. *Addit Manuf* 2015;8:12–35. <https://doi.org/10.1016/j.addma.2015.07.002>.
- [5] Muhammad M, Gusain R, Ghiaasiaan SR, Gradl PR, Shao S, Shamsaei N. Microstructure and Mechanical Properties of Additively Manufactured Haynes 230: A Comparative Study of L-PBF vs. LP-DED 2022. <https://doi.org/10.26153/TSW/44174>.
- [6] Poudel A, Yasin MS, Ye J, Liu J, Vinel A, Shao S, et al. Feature-based volumetric defect classification in metal additive manufacturing. *Nature Communications* 2022 13:1 2022;13:1–12. <https://doi.org/10.1038/s41467-022-34122-x>.
- [7] Nandi I, Shamsaei N, Shao S. Investigating the effect of defects on the crack initiation of additively manufactured IN718 using crystal plasticity simulations 2022. <https://doi.org/10.26153/TSW/44170>.

- [8] Muhammad M, Gusain R, Ghiaasiaan SR, Gradl PR, Shao S, Shamsaei N. Microstructure and Mechanical Properties of Additively Manufactured Haynes 230: A Comparative Study of L-PBF vs. LP-DED 2022. <https://doi.org/10.26153/TSW/44174>.
- [9] Ahmad N, Ghiaasiaan R, Gradl PR, Shao S, Shamsaei N. Low cycle fatigue behavior of additively manufactured Haynes 282: Effect of post-processing and test temperature. *Int J Fatigue* 2023;176:107880. <https://doi.org/10.1016/j.ijfatigue.2023.107880>.
- [10] Ahmad N, Ghiaasiaan R, Gradl PR, Shao S, Shamsaei N. Revealing deformation mechanisms in additively manufactured Alloy 718: Cryogenic to elevated temperatures. *Materials Science and Engineering: A* 2022;849:143528. <https://doi.org/10.1016/J.MSEA.2022.143528>.
- [11] Avula I, Arohi AC, Kumar CS, Sen I. Microstructure, Corrosion and Mechanical Behavior of 15-5 PH Stainless Steel Processed by Direct Metal Laser Sintering. *J Mater Eng Perform* 2021;30:6924–37. <https://doi.org/10.1007/S11665-021-06069-5/FIGURES/5>.
- [12] Sarkar S, Kumar CS, Nath AK. Effects of heat treatment and build orientations on the fatigue life of selective laser melted 15-5 PH stainless steel. *Materials Science and Engineering: A* 2019;755:235–45. <https://doi.org/10.1016/J.MSEA.2019.04.003>.
- [13] Croccolo D, De Agostinis M, Fini S, Olmi G, Bogojevic N, Ciric-Kostic S. Effects of build orientation and thickness of allowance on the fatigue behaviour of 15–5 PH stainless steel manufactured by DMLS. *Fatigue Fract Eng Mater Struct* 2018;41:900–16. <https://doi.org/10.1111/FFE.12737>.
- [14] Lee JR, Lee MS, Chae H, Lee SY, Na T, Kim WS, et al. Effects of building direction and heat treatment on the local mechanical properties of direct metal laser sintered 15-5 PH stainless steel. *Mater Charact* 2020;167:110468. <https://doi.org/10.1016/J.MATCHAR.2020.110468>.
- [15] Guo C, Hu R, Chen F. Microstructure and performances for 15-5 PH stainless steel fabricated through the wire-arc additive manufacturing technology. <https://doi.org/10.1080/1066785720201800296> 2020;36:831–42. <https://doi.org/10.1080/10667857.2020.1800296>.
- [16] Roberts D, Zhang Y, Charit I, Zhang J. A comparative study of microstructure and high-temperature mechanical properties of 15-5 PH stainless steel processed via additive manufacturing and traditional manufacturing. *Progress in Additive Manufacturing* 2018;3:183–90. <https://doi.org/10.1007/S40964-018-0051-5/FIGURES/9>.
- [17] Chae H, Luo MY, Huang EW, Shin E, Do C, Hong SK, et al. Unearthing principal strengthening factors tuning the additive manufactured 15-5 PH stainless steel. *Mater Charact* 2022;184:111645. <https://doi.org/10.1016/J.MATCHAR.2021.111645>.
- [18] Croccolo D, Bogojević N, De Agostinis M, Fini S, Olmi G, Robusto F, et al. Fatigue response of additively manufactured as-built 15-5 PH stainless steel and effects of machining and thermal and surface treatments. *Fatigue Fract Eng Mater Struct* 2023;46:433–51. <https://doi.org/10.1111/FFE.13875>.
- [19] Nezhadfar PD, Gradl PR, Shao S, Shamsaei N. Microstructure and Deformation Behavior of Additively Manufactured 17–4 Stainless Steel: Laser Powder Bed Fusion vs. Laser Powder Directed Energy Deposition. *JOM* 2022;74:1136–48. <https://doi.org/10.1007/S11837-021-05032-Y/FIGURES/9>.
- [20] Peng X yuan, Zhou X liang, Hua X zhen, Wei Z wei, Liu H ying. Effect of Aging on Hardening Behavior of 15-5 PH Stainless Steel. *Journal of Iron and Steel Research International* 2015;22:607–14. [https://doi.org/10.1016/S1006-706X\(15\)30047-9/METRICS](https://doi.org/10.1016/S1006-706X(15)30047-9/METRICS).
- [21] Li Q, Zhang TW, Qiao JW, Ma SG, Zhao D, Lu P, et al. Superior tensile properties of Al_{0.3}CoCrFeNi high entropy alloys with B₂ precipitated phases at room and cryogenic temperatures. *Materials Science and Engineering: A* 2019;767:138424. <https://doi.org/10.1016/J.MSEA.2019.138424>.